Nanoelectromechanical systems

K. L. Ekinci[a)]
Department of Aerospace & Mechanical Engineering, Boston University, Boston, Massachusetts 02215

M. L. Roukes[b)]
Departments of Physics, Applied Physics, and Bioengineering, California Institute of Technology, 114-36, Pasadena, California 91125

(Received 8 December 2004; accepted 16 April 2005; published online 26 May 2005)

Nanoelectromechanical systems (NEMS) are drawing interest from both technical and scientific communities. These are electromechanical systems, much like microelectromechanical systems, mostly operated in their resonant modes with dimensions in the deep submicron. In this size regime, they come with extremely high fundamental resonance frequencies, diminished active masses, and tolerable force constants; the quality (Q) factors of resonance are in the range $Q \sim 10^3 - 10^5$—significantly higher than those of electrical resonant circuits. These attributes collectively make NEMS suitable for a multitude of technological applications such as ultrafast sensors, actuators, and signal processing components. Experimentally, NEMS are expected to open up investigations of phonon mediated mechanical processes and of the quantum behavior of mesoscopic mechanical systems. However, there still exist fundamental and technological challenges to NEMS optimization. In this review we shall provide a balanced introduction to NEMS by discussing the prospects and challenges in this rapidly developing field and outline an exciting emerging application, nanoelectromechanical mass detection. © *2005 American Institute of Physics.* [DOI: 10.1063/1.1927327]

I. INTRODUCTION

Using the materials and processes of microelectronics, researchers have long been fashioning microscopic machines—beams, cantilevers, gears, and membranes. These mechanical elements and the microelectronic circuits that control them are generally referred to as microelectromechanical systems (MEMS). MEMS have been deployed to perform mundane tasks in present day technology—such as opening and closing valves, turning mirrors, regulating electric current, or light flow. Today, numerous companies, from the semiconductor giants to fledgling startups, are making MEMS devices for a wide range of consumers. With microelectronics technology now pushing deep into the submicron, time is ripe to embark upon a concerted exploration of nanoelectromechanical systems (NEMS).[1,2]

Figure 1 shows a family of semiconductor NEMS and outlines their generic fabrication steps. This process for patterning freely suspended nanometer scale semiconductor structures is referred to as surface nanomachining—as opposed to the bulk micromachining of MEMS. These techniques apply to silicon on insulator structures,[3] gallium arsenide/aluminum arsenide (GaAs/AlGaAs) systems,[4] silicon carbide (SiC) on silicon,[5] aluminum nitride on silicon,[6] nanocrystalline diamond films,[7] and amorphous silicon nitride films.[8] Most of these materials are available with high purity, grown with a precise control of the layer thicknesses. This latter aspect yields dimensional control in the vertical (out-of-plane) dimension at the monolayer level. This is nicely compatible with the lateral dimensional precision of electron beam lithography that approaches the atomic scale.

NEMS have a host of intriguing attributes. They offer access to a parameter space that is unprecedented: fundamental resonance frequencies in the microwaves,[9] mechanical quality (Q) factors in the tens of thousands,[10] active masses in the femtograms, heat capacities far below a yocto calorie[11]—this list goes on. These attributes spark the imagination, and a flood of ideas for exciting experiments and applications ensues—but a multitude of unanticipated questions and concerns accompanies: How shall transducers be realized at the nanoscale? How shall surface properties be controlled? How can reproducible nanofabrication be attained? To what extent can continuum theory be pushed into the nanoregime to describe the mechanics of NEMS? Clearly, the characteristic parameters of NEMS are extreme by any measure. Those who would develop the next generation NEMS must advance into the frontiers of physics and engineering in several directions at once.

This review is in four main sections. In the following two sections, we shall attempt to convey a balanced introduction to NEMS. We shall not only discuss the exciting attributes of NEMS, but also give a survey of the existing technological and fundamental challenges in the field. As we move forward, it will become increasingly apparent which of these challenges will be negotiable through systematic engineering, and what hard, immutable limits are imposed by the fundamental laws of nature. In the fourth section of this article, we shall touch upon an emerging exciting application

a)Author to whom correspondence should be addressed; electronic mail: ekinci@bu.edu
b)Electronic mail: roukes@caltech.edu

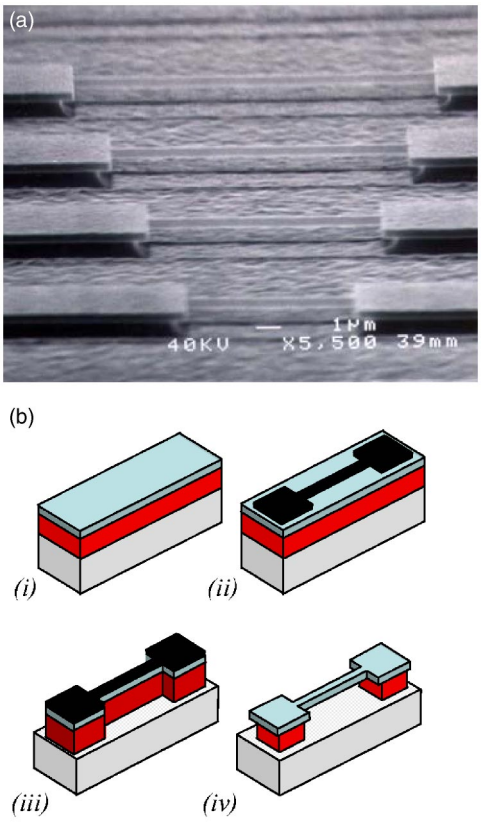

FIG. 1. (Color online). (a) Scanning electron micrograph of SiC NEMS. This first family of submicron doubly clamped beams exhibits fundamental flexural resonant frequencies from 2 to 134 MHz. They were patterned at Caltech from 3C–SiC epilayers grown at Case Western Reserve University (see Ref. 5). (b) Surface nanomachining of NEMS. Fabrication starts on a semiconductor heterostructure such as the one shown in (i) with structural (top) and sacrificial (middle) layers on top of a substrate (bottom). (ii) First an etch mask is defined via electron beam lithography. (iii) Then, the pattern is transferred into the sacrificial layer using an anisotropic etch such as a plasma etch. (iv) Finally, the sacrificial layer under the structure is removed using a selective etch. The structures can be metallized after or during the process depending upon the specific measurement requirements.

of NEMS: ultrasensitive nanoelectromechanical mass detection.[12] In Sec. V we present our projections.

II. NEMS ATTRIBUTES

A. NEMS as multiterminal electromechanical devices

Figure 2 depicts a generic multiterminal electromechanical device, where electromechanical transducers provide input mechanical stimuli to the system, and read out its mechanical response. At additional control terminals, electrical signals—either quasistatic or time varying—can be applied, and subsequently be converted by the control transducers into forces to perturb the properties of the mechanical element.

NEMS devices fit the above-described general portrayal. We can further classify the existing NEMS as resonant and quasistatic. In this review, our focus will primarily be on the so-called resonant devices as most initial NEMS applications involve these. The input transducers in resonant NEMS convert electrical energy into mechanical energy by exciting a resonant mode of the mechanical element. The mechanical response, namely the displacement of the element, is transduced back into electrical signals. In the resonant mode of operation, external perturbations can be regarded as the control signals, since they modify the vibrational characteristics, such as the resonance frequency $\omega_0/2\pi$ or the Q of the vibrating element. We shall discuss electromechanical transduction mechanisms in NEMS and give examples of measurements of external perturbations in Sec. IV.

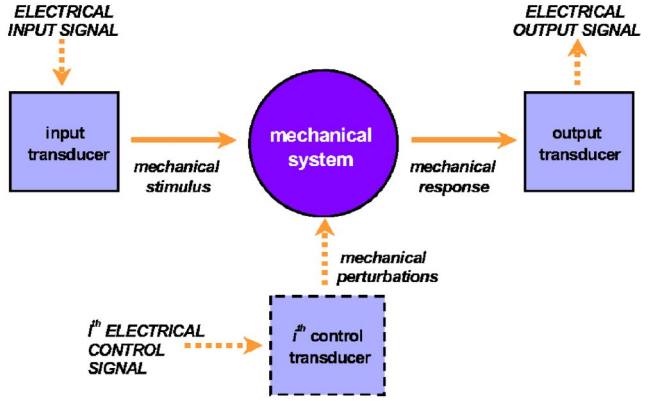

FIG. 2. (Color online). Schematic representation of a multiterminal electromechanical device.

B. Frequency

In Fig. 3, we have plotted the experimentally attained frequencies for the fundamental flexural modes of thin beams, for dimensions spanning the domain from MEMS to deep within NEMS.[5,9] Continuum mechanics approximations appear to hold, i.e., the expression $\omega_0/2\pi = (1.05)\sqrt{E/\rho}(t/l^2)$ determines the flexural resonance frequencies of thin doubly clamped NEMS beams.[13] Here, $w \times t \times l$ are the dimensions, E is the Young's modulus, and ρ is the mass density of the beam (Fig. 3 inset). It is particularly notable that for structures of the same dimensions, Si yields frequencies of a factor of 2, and SiC a factor of three

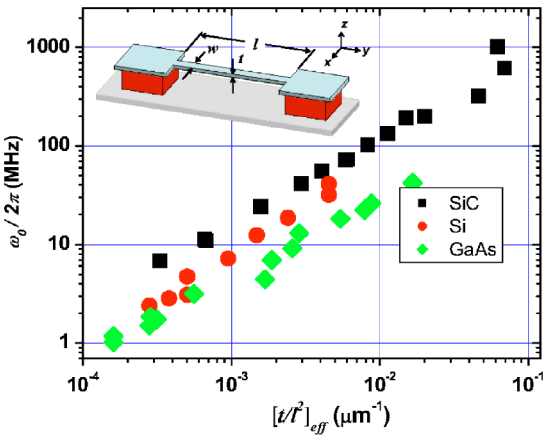

FIG. 3. (Color online). Frequency versus effective geometry for doubly clamped beams made from single-crystal SiC, Si, and GaAs (see Refs. 5 and 9). The inset shows the doubly clamped beam geometry with length l, width w, and thickness t. The fundamental out-of-plane (in-plane) flexural resonance frequency of this structure is given by the expression, $\omega_0/2\pi = 1.05\sqrt{E/\rho}(t/l^2)$ ($\omega_0/2\pi = 1.05\sqrt{E/\rho}(w/l^2)$). In the plot, t/l^2 values have been normalized to remove the effect of additional stiffness and mass loading due to electrode metallization.

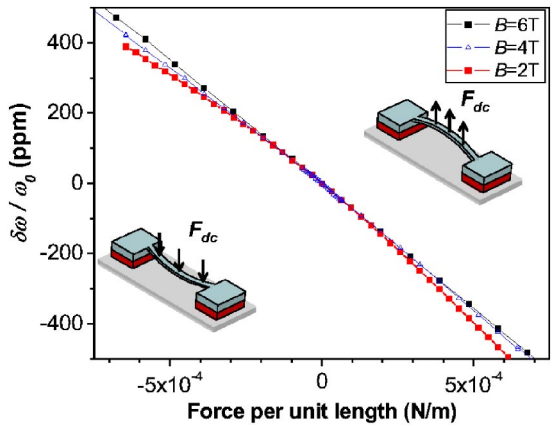

FIG. 4. (Color online). Measurements of internal strain in doubly clamped nanomechanical beam resonators. Here, the beam is subjected to a static force F_{dc} in addition to a small ac excitation force around the resonance frequency ω_0. The net effect is a shift $\delta\omega$ in ω_0. F_{dc} was generated by passing a dc current I_{dc} along the length of the beam in a static magnetic field. The frequency shift data $\delta\omega/\omega_0$ are plotted against F_{dc} per the beam's unit length $I_{dc}B$ for three different magnetic field strengths B. The apparent curvature at the lowest field value of $B=2$ T, can be attributed to heating effects since to obtain the same F_{dc}, a larger I_{dc} is required at lower B. A simple analysis using elasticity theory indicates that $\delta\omega$ is positive and symmetric around $F_{dc}=0$ in an unstrained beam resonator. A resonator with an internal strain, however, exhibits a sign change in $\delta\omega/\omega_0$—consistent with the displayed data.

higher than those obtained with GaAs devices. This increase reflects the increased phase velocity $\sqrt{E/\rho}$ in the stiffer materials.

Of course, even smaller sizes than this will ultimately become feasible—especially for nanowire[14,15] and nanotube[16] NEMS. One might ask at what size scale does continuum mechanics break down and corrections from atomistic behavior emerge? Molecular dynamics simulations[17,18] for ideal structures and initial experiments[19] appear to indicate that this becomes manifested only for structures on the order of tens of lattice constants in cross section. Hence, for most current work in NEMS, continuum approximations appear to be adequate.

In most NEMS, especially in bilayer or multilayer structures (common for devices that include transducers), internal strains must be taken into account when estimating resonance frequencies. Figure 4 depicts our initial efforts to characterize such effects in semiconductor NEMS with metallization overlayers. In these measurements, small static forces were applied to doubly clamped nanomechanical beam resonators and their resonance frequencies were tracked as a function of the applied force. The induced frequency shifts, especially the apparent directionality associated with the shift, are consistent with the existence of a residual internal strain.

C. Quality (Q) factor

The Q factors attained to date in semiconductor NEMS are in the range 10^3–10^5. This greatly exceeds those typically available from electrical oscillators. This small degree of internal dissipation imparts to NEMS their low operating power levels and high attainable sensitivities as we shall discuss in more detail in the next subsection. For signal processing devices, high Q directly translates into low insertion loss.[20] It is important to note that large Q does imply a reduction of bandwidth, yet this need not be deleterious to performance for two reasons. First, feedback control, which can be applied without introduction of significant additional noise, may be useful to increase bandwidth as desired.[21–23] Second, for resonators operating at ~1 GHz, even in the case of extremely high Q of $\sim 10^5$, bandwidths of ~10 kHz will be obtainable; this is already sufficient for various narrow band applications.

D. Characteristic operating power level

A rough understanding of the minimum operating power level P_{min} for a resonant NEMS device can be reached by realizing that the resonator simply is a lossy energy storage device. Energy pumped into the device is dissipated in a time interval $\tau \sim Q/\omega_0$ called the ring-up or ring-down time of the resonator. We define the minimum operation energy for the system as the energy, which will drive the system at amplitudes comparable to those of the thermal fluctuations. Given the energy k_BT of thermal fluctuations in the mode, the minimum input power can be estimated as

$$P_{min} \sim k_B T \omega_0 / Q. \quad (1)$$

For NEMS device dimensions accessible today via electron beam lithography, the characteristic minimum power level is on the order of 10 aW (10^{-17} W). Even if we multiply this by a factor of 1 000 000, to achieve robust signal-to-noise ratios, and then further envision a million such devices acting in concert to realize some sort of future NEMS-based mechanical signal processing or computation system, the total system power levels are still only on the order of 1 μW. This is 6 orders of magnitude smaller than the power dissipation in current systems of similar complexity based upon digital devices that work solely in the electronic domain.

E. Responsivity

It is possible to employ existing micron-scale MEMS technology to attain high frequencies. This approach, however, has serious disadvantages, which preclude realization of the full scope of potentialities offered by NEMS technology. To illustrate this we shall again focus our discussion on doubly clamped beams, with aspect ratios l/w or l/t. Attainment of high frequencies with micron-scale structures can only occur with foreshortened aspect ratios of order unity. Such geometries yield extremely high force constants κ_{eff}. Large κ_{eff} could adversely affect: (a) the attainable dynamic range, (b) the ability to tune the devices using "control" signals (applied mechanical forces), (c) the attainment of maximum Q (through minimization of acoustic radiation to the support structures, i.e., clamping losses), and (d) the excitation levels required to induce nonlinear response. All of these characteristics are optimized in large aspect ratio structures, i.e., structures with geometries currently used in MEMS, but with all dimensions reduced to nanoscale dimensions: NEMS. Calculated κ_{eff} and other important parameters for several NEMS along with their dimensions are presented in Table I.

TABLE I. Important attributes for a family of doubly clamped Si beams with $Q=10\,000$ at $T=300$ K. The effective force constant $\kappa_{\text{eff}}=32Et^3w/l^3$ is defined for point loading at the beam's center. Nonlinear onset amplitude $\langle x_c\rangle$ has been characterized using the criterion described in the text. The thermomechanically limited linear dynamic range (DR) is calculated for the natural bandwidth of the beam $\Delta f\approx\omega_0/2\pi Q$ and $\text{DR}=20\log(\langle x_c\rangle/\langle x_{\text{th}}\rangle)$, where $\langle x_{\text{th}}\rangle=(k_BT/\kappa_{\text{eff}})^{1/2}$. Effective mass for the fundamental mode is $M_{\text{eff}}\approx 0.73M_{\text{tot}}$ where M_{tot} is the total mass of the beam.

$w\times t\times l$	$\omega_0/2\pi$ (MHz)	κ_{eff} (N/m)	$\sqrt{S_x^{(\text{th})}(\omega_0)}$ (nm/$\sqrt{\text{Hz}}$)	$\langle x_c\rangle$ (nm)	Thermomechanically limited linear DR for $\Delta f\sim\omega_0/Q$ (dB)	M_{eff} (g)
150 nm×400 nm×17.5 μm	10	~8	5.7×10^{-4}	8	~50	1.8×10^{-12}
100 nm×200 nm×2 μm	385	~480	6.5×10^{-5}	4	~62	9.3×10^{-14}
50 nm×80 nm×0.78 μm	1000	~290	1.0×10^{-5}	1.6	~52	5.3×10^{-15}

F. Available dynamic range

The linear dynamic range (DR) is a widely used concept in amplifier characterization, expressing the window of input power in which the amplifier behaves linearly. The bottom of the DR is determined by the noise power generated within the amplifier (referred back to its input), and the top by the (input) power level at which 1 dB compression occurs.

Similarly, we shall attempt to define a DR for a NEMS resonator as the ratio of its maximum vibration amplitude (at the onset of nonlinearity) to its rms displacement noise floor within the operation bandwidth Δf. In general, a NEMS resonator is always followed by a transducer-amplifier cascade. In most narrowband operation, Δf is determined by this transducer-amplifier cascade. One might sometimes desire to use the entire resonant response in which case the measurement bandwidth becomes the natural (noise) bandwidth of the resonator $\Delta f\approx\omega_0/2\pi Q$.

The block diagram for a generic NEMS resonator operated in its fundamental mode and coupled to a noisy transducer-amplifier cascade is shown in Fig. 5. The mechanical response for the fundamental mode of the resonator can be approximated by that of a one-dimensional damped harmonic oscillator with the following parameters: an effective mass M_{eff}; an effective force constant (stiffness) $\kappa_{\text{eff}}=M_{\text{eff}}\omega_0^2$; and a quality factor Q. The transfer function $G(\omega)$ for the resonator then becomes

$$G(\omega)=\frac{1}{M_{\text{eff}}(\omega_0^2-\omega^2+i\omega\omega_0/Q)}. \tag{2}$$

To retain the generality of the discussion, we shall assume that the resonator is driven by a noiseless drive force at $\omega=\omega_0$, a dominant intrinsic noise and by the backaction force of the transducer–amplifier. The drive has a force spectral density $\langle x_d\rangle^2\ \delta(\omega-\omega_0)/|G(\omega_0)|^2$. $\langle x_d\rangle$ is the rms vibration amplitude to which the resonator is driven and $\langle x_d\rangle$ is assumed to be within the linear regime of the resonator. The power spectral density $S_F^{(i)}(\omega)$ (with units N^2/Hz) of the intrinsic force noise term is determined by the dominant physical noise mechanism. We shall have more to say about intrinsic noise sources in NEMS in Sec. III B. $S_F^{(b)}(\omega)$ quantifies the force noise resulting from the backaction of the transducer–amplifier cascade. The backaction force[24] represents the reverse coupling and drives the mechanical element as electrical impulses are generated in the transducer–amplifier cascade.

Apparently, the displacement noise floor, hence, the DR of the NEMS–transducer–amplifier cascade of Fig. 5 will be determined by the larger of the two distinct classes of mechanisms—intrinsic noise processes fundamental to the nanomechanical resonator itself[25,26] or extrinsic processes that originate from the transducer–amplifier circuitry.[27] We now obtain general expressions for the displacement noise floor due to each process. The noise in the drive force generates the rms displacement noise,

$$\left[\int_{2\pi\Delta f}[S_F^{(i)}(\omega)+S_F^{(b)}(\omega)]|G(\omega)|^2d\omega\right]^{1/2}.$$

Similarly, the voltage noise generated within the transducer–amplifier cascade with (white) spectral power density $S_V(\omega)$ appears as a displacement noise at the input of the cascade with an rms magnitude

$$\left[\int_{2\pi\Delta f}\frac{S_V(\omega)}{\Re^2}d\omega\right]^{1/2}.$$

Here, $\Re=\partial V/\partial X$ is the cascade responsivity (with units V/m).

A very important conclusion can be reached based upon the above discussion: the bottom segment of the available DR will be forfeited unless optimal transducer–amplifier cascades are employed to read out the NEMS motion. To utilize the full potential of NEMS, displacement transduction schemes are required that can provide resolution at the level of the intrinsic displacement fluctuations without introducing significant backaction noise.

When extremely low noise transducer–amplifiers are available, the operation limits are usually set by the thermomechanical displacement fluctuations in the mechanical element. In Table I, we present the thermomechanical noise levels for representative NEMS. $S_X^{(\text{th})}(\omega_0)$ is obtained[23] by setting $S_F^{(i)}(\omega)=4M_{\text{eff}}\omega_0k_BT/Q$ and evaluating $S_X^{(\text{th})}(\omega_0)=S_F^{(i)}(\omega_0)|G(\omega_0)|^2$.

Having established the noise floor or the bottom end of the DR, we turn to the top end. The top end will be determined by the critical drive amplitude $\langle x_c\rangle$ at the onset of nonlinearity. The source of nonlinearities in mechanical systems can be geometric, inertial, or material in nature. Therefore, to establish this power level requires specific knowledge of the device geometry and the dominant mechanism for nonlinear behavior in the device material.[28,29] In the doubly clamped beam geometry, for instance, for $\langle x_d\rangle>\langle x_c\rangle$ near

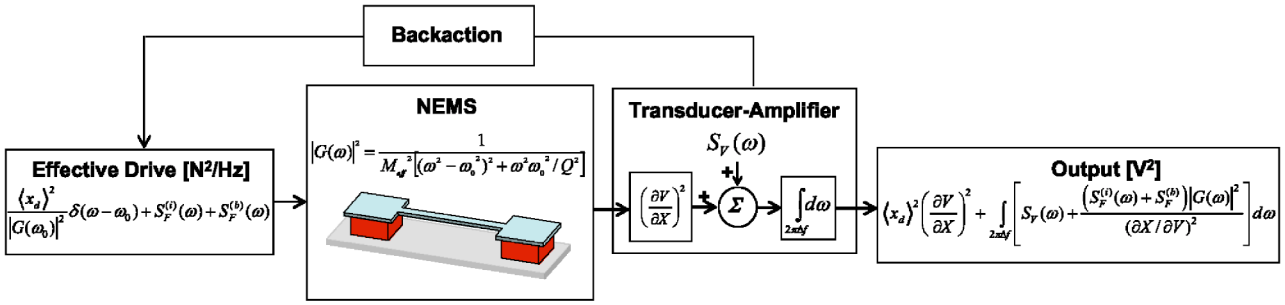

FIG. 5. (Color online). Block diagram of a NEMS–transducer–amplifier cascade. In the noise analysis, the nanomechanical resonator is assumed to respond to a drive force localized at $\omega=\omega_0$, an intrinsic force noise, and the backaction force noise of the transducer. The resonator's mechanical response is characterized by its (linear, one-dimensional) transfer function $G(\omega)$. The resonator converts the input drive force into a displacement and subsequently, the (linear) transducer–amplifier converts this displacement into an electrical voltage. We assume that the transducer–amplifier cascade is noisy and has a displacement responsivity $\partial V/\partial X$. At the output of the cascade, all the noise power as well as the drive force is converted to a voltage and integrated over the measurement bandwidth Δf. Note that for the DR calculation, one can convert all the signals to a displacement (referred to as the input of the transducer–amplifier) or to a voltage (referred to as the output of the transducer–amplifier).

$\omega \approx \omega_0$, the flexure causes the beam to lengthen adding a significant correction to the elastic response.[28] This condition translates into the relation

$$\langle x_c \rangle \approx \left[\frac{2}{0.528Q(1-\sigma^2)} \right]^{1/2} t, \tag{3}$$

which depends upon the beam's thickness t in the direction of vibration as well as its Poisson's ratio σ and Q.[15,30] We note that for a cantilever, a similar formulation based upon a single dominant effect cannot be made.[31] The onset of nonlinearity based upon the aforementioned criterion in doubly clamped beams is displayed in Table I for the representative devices.

With these limits, the DR within the operation bandwidth Δf becomes

$$\mathrm{DR} = 10 \log \left[\langle x_c \rangle^2 / \int_{2\pi\Delta f} S_X^{(\mathrm{eff})}(\omega) d\omega \right]. \tag{4}$$

Here, $S_X^{(\mathrm{eff})}(\omega)$ is the effective noise floor within Δf, i.e., the larger of $S_V(\omega)/\Re^2$ or $[S_F^{(i)}(\omega)+S_F^{(b)}(\omega)]|G(\omega)|^2$. In Table I, we have calculated thermomechanically limited DR values for $\Delta f \approx \omega_0/2\pi Q$.

We conclude this section by noting that nonlinear behavior is not only desirable in certain applications[14,32–34] such as in signal processing but also contains a plethora of interesting physics.[35,36]

G. Active mass

Only a fraction of the total resonator's mass is involved in its motion. For beams or cantilevers, multiplying the total mass by the integral of a normalized function describing the modal shape yields a measure of the active mass M_{eff}. For a doubly clamped beam operating in fundamental mode, for instance, $M_{\mathrm{eff}} \approx 0.73 M_{\mathrm{tot}}$, where M_{tot} is the total mass of the beam.[37] We display M_{eff} for the representative NEMS in Table I.

We shall discuss the implications of the minuscule M_{eff} of NEMS in Sec. III when considering phase noise issues, reproducible nanofabrication, and NEMS based mass detection.

III. PRINCIPAL CHALLENGES

A. Pursuit of ultrahigh *Q*

Central to attaining the ultimate limits of NEMS performance is the pursuit of ultrahigh Q. This overarching theme underlies almost all fundamental and applied research in NEMS. From an applications point of view, dissipation $(\sim 1/Q)$ within a resonant mechanical element: (a) limits its sensitivity to externally applied forces (signals), (b) sets the level of fluctuations that degrade its spectral purity (i.e., broaden its natural linewidth), and (c) determines the minimum intrinsic power levels at which the device must operate. Ultrahigh Q, therefore, is the performance limiting aspect in a number of important applications: in low phase noise oscillators such as those required in timekeeping;[27,38] in highly selective filters[39] for signal processing; and in resonant sensors[40,41] where resonance frequency shifts are tracked due to external perturbations (see Sec. IV). We hasten to add that energy dissipation in mesoscopic mechanical systems is an interesting problem of fundamental importance on its own.

Extrinsic and intrinsic mechanisms are operative to limit Q in real NEMS devices. In this review, we shall present a short survey of some of these intrinsic and extrinsic loss mechanisms rather than lengthy discussions. The interested reader can find the more complete considerations in the cited references.

We start with extrinsic sources. Several of these sources have been investigated in some detail. These include: (a) losses due to gas damping, (b) clamping losses at supports, and (c) coupling losses mediated through transducers.

In Fig. 6, we present our recent measurements of the effect of a surrounding gas on a NEMS resonator. At very low pressures—in the so-called molecular regime, where the mean free path of the gas molecules is much larger than the device dimensions—the resonator dissipates energy through collisions with individual molecules. Using simple arguments,[42–45] a quality factor due to the gas dissipation can be determined as $Q_{\mathrm{gas}} \approx M_{\mathrm{eff}}\omega_0 \upsilon / pA$. Here, $\upsilon = \sqrt{k_B T/m}$ is the thermal velocity of the gas molecules each with mass m, p is the surrounding the gas pressure, and A is the surface area of the resonator. The so-called loaded Q of the device can then be determined as $Q_L = (Q_i^{-1} + Q_{\mathrm{gas}}^{-1})^{-1}$, where Q_i is the intrinsic

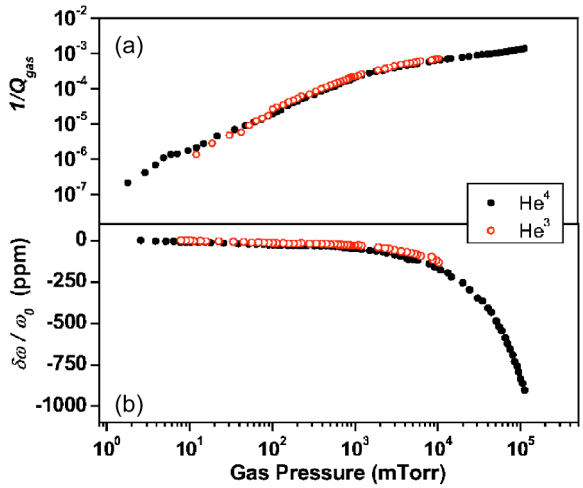

FIG. 6. (Color online). Effect of surrounding gas pressure upon the resonance parameters of a GaAs doubly clamped NEMS beam with $\omega_0/2\pi \approx 4.38$ MHz. The intrinsic Q of the device was $Q_i \approx 10^4$. Q_L and $\delta\omega$ of the beam were measured as a function of the gas pressure in the measurement chamber. Q_{gas} was later extracted using Q_i. The measurement was done with He^3 and He^4 gases. Note the crossover in the plots from the ideal gas regime to the viscous regime.

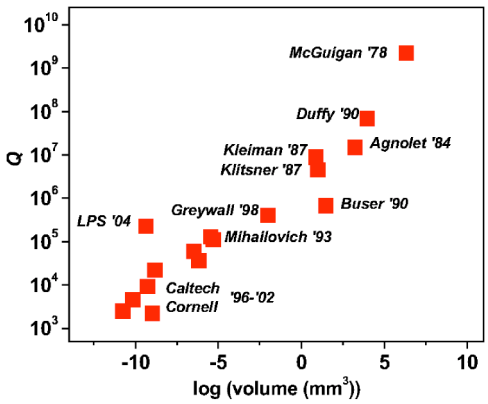

FIG. 7. (Color online). Maximum reported Q factors in monocrystalline mechanical resonators varying in size from the macroscale to nanoscale. The data follow a trend showing a decrease in Q factor that occurs roughly with linear dimension, i.e., with increasing volume-to-surface ratio.

Q. In Fig. 6(a), we plot Q_{gas}^{-1} as a function of p. At low p, Q_{gas}^{-1} depends linearly on p. At high p, a crossover into a viscous dissipation regime[46] is apparent; $Q_{\text{gas}}^{-1} \propto p^{1/2}$. The same crossover is also manifest in the resonance frequency shift, $\delta\omega/\omega_0$, displayed in Fig. 6(b). In the molecular regime, negligible frequency shift is observed; in the viscous regime, mass loading reduces ω_0. This crossover pressure can be determined by comparing the sound wavelength in the medium to the mean free path of the gas molecules.[47]

A resonator can lose the energy in its resonant modes via the acoustic coupling to its clamps.[48–50] Most high frequency NEMS have been realized in the doubly clamped beam configuration (see Fig. 3). One of the possible reasons for the decrease of Q factor in these devices is the clamping loss intrinsic to the doubly clamped boundary condition. Recent demonstration of augmented clamping loss in doubly clamped NEMS beam resonators agrees with this claim. Huang *et al.*[51] have compared the Q factor from identical nanomechanical beams with free–free and doubly clamped boundary conditions, clearly showing a ~2.5-fold enhancement in the Q of the free–free beam.

The possibility exists that displacement transduction process itself may contribute to the dissipation,[52,53] causing apparent changes in the observed Q—sometimes also called the loaded Q, Q_L. Cleland and Roukes,[52] for instance, quantified the contribution of the magnetomotive transduction circuitry to the observed dissipation in NEMS. They developed a technique whereby the external electrical damping could be measured and controlled locally, enabling the manipulation of Q_L.

In looking at intrinsic dissipation sources, it is essential to discriminate between energy dissipation that occurs in a perfect crystal lattice and energy dissipation that occurs in a real, imperfect crystal with bulk and surface defects. The loss mechanisms in a perfect crystal are fundamental. These impose the ultimate upper bounds to attainable Qs; such processes include thermoelastic damping arising from anharmonic coupling between mechanical modes and the phonon reservoir,[54] and losses due to electron–phonon and phonon–phonon interactions. The intrinsic mechanisms due to imperfections in the crystal may be suppressed by careful choice of materials, processes, and handling. These include anelastic losses involving defects in the bulk[55,56] and surfaces.

NEMS devices patterned from single crystal, ultrapure heterostructures can contain very few (even zero) crystallographic defects and impurities. Hence, the initial hope was that within small enough structures bulk acoustic energy loss processes should be suppressed and ultrahigh Q factors thereby attained. Surprisingly, to date, a wide collection of NEMS resonators—fabricated from different materials and processed using different surface nanomachining techniques—have yielded relatively low Q factors in the 10^3–10^5 range.

There is overwhelming experimental evidence that surfaces contribute to the energy dissipation in NEMS in a dominant fashion. Surface treatment experiments in ultrahigh vacuum (UHV) on nano- and micromechanical devices have shown that surface oxides, defects, and adsorbates augment the energy dissipation. Annealing nanometrically thin Si cantilevers in UHV,[57,58] for instance, increased their Q factors by 1 order of magnitude. In subsequent x-ray photoelectron spectroscopy experiments,[59,60] removal of oxygen from nanoscale cantilever surfaces was correlated with improvements in the mechanical Q factor. More recently, methyl monolayers were shown to suppress dissipation in silicon micromechanical devices.[61] Figure 7 displays the rough trend that seems to be manifest in mechanical resonators in general—from those that are truly macroscopic in size, to those well within the domain of NEMS. The maximum attainable Qs seem to scale downward with linear dimension, i.e., volume-to-surface ratio. We note that the Q measurements in resonators compiled in Fig. 7 were done at different temperatures.[62–68,3,2,69]

Given what is known from electronic and photonic device physics regarding oxidation and reconstruction of the Si surface, it seems clear that the mechanical properties of the smallest NEMS devices will deviate greatly from those in

TABLE II. Expressions for NEMS phase noise $S_\omega(\omega)$ and frequency fluctuations $\delta\omega_0$ for different noise mechanisms. $\delta\omega_0$ are given for a measurement bandwidth Δf. The resonator is assumed to be driven to its critical drive amplitude $\langle x_c\rangle$ characterized by an energy $E_c = M_{\text{eff}}\omega_0^2\langle x_c^2\rangle$. In the first row, the (white) voltage noise generated in the transducer–amplifier cascade is the dominant noise source; the symbols used have been defined in Sec. II F. The DR here is amplifier limited, and $\text{DR} = 10\log[\langle x_c\rangle^2/(S_V\Delta f/\Re^2)]$. In the second row, we present frequency fluctuations due to thermomechanical noise. Here, the measurement scheme effectively determines $S_\omega(\omega)$, although the obtained $\delta\omega_0$ is scheme independent. In the third row, temperature fluctuations are considered. Here, c_s is the temperature dependent speed of sound; $\alpha_T = (1/l)\partial l/\partial T$ is the linear thermal expansion coefficient; and g and τ_T are the thermal conductance and the thermal time constant for the nanostructure, respectively. In the fourth row, the noise presented arises from the adsorption–desorption of gas molecules upon the resonator. To determine the adsorption–desorption noise, the surface is modeled as comprising N_a sites for the adsorption of molecules of mass m with σ_{occ}^2 representing the variance in the occupation probability of a site; τ_r is the correlation time for an adsorption–desorption cycle. In the bottom row, the momentum exchange noise from impinging gas molecules has been calculated for the low pressure limit with the parameters defined in Sec. III A.

Type of noise	$S_\omega(\omega)$	$\delta\omega_0$
Amplifier[a,b]	$\omega_0^2 S_V(\omega)/Q^2\Re^2\langle x_c\rangle^2$	$(\omega_0/Q)10^{-(\text{DR}/20)}$
Thermomechanical[a,c]	$(\omega_0^5/Q^3)(k_BT/E_C)[1/(\omega^2-\omega_0^2)^2+\omega^2\omega_0^2/Q^2]$ (PLL) $k_BT\omega_0/E_cQ$ (self-excited loop)	$\omega_0(k_BT/E_c)^{1/2}(\Delta f/Q\omega_0)^{1/2}$
Temperature fluctuations[c]	$[(-22.4c_s^2/\omega_0^2l^2)\alpha_T+(2/c_s)(\partial c_s/\partial T)]^2[\omega_0^2k_BT^2/\pi g(1+(\omega-\omega_0)^2\tau_T^2)]$	$\omega_0/\pi^{1/2}[(-22.4c_s^2/\omega_0^2l^2)\alpha_T+(2/c_s)(\partial c_s/\partial T)]\times[k_BT^2\arctan(2\pi\Delta f\tau_T)/g\tau_T]^{1/2}$
Adsorption–desorption[c–e]	$\{2\pi\omega_0^2N_a\sigma_{\text{occ}}^2\tau_r/[1+(\omega-\omega_0)^2\tau_r^2]\}(m/M_{\text{eff}})^2$	$\omega_0 m/M_{\text{eff}}\sigma_{\text{occ}}[N_a\arctan(2\pi\Delta f\tau_r)]^{1/2}$
Momentum exchange[f,g]	$(\omega_0^5/Q_{\text{gas}}^3)(k_BT/E_C)[1/(\omega^2-\omega_0^2)^2+\omega^2\omega_0^2/Q_{\text{gas}}^2]$ (PLL) $k_BT\omega_0/E_cQ_{\text{gas}}$ (self-excited loop)	$\omega_0(k_BT/E_c)^{1/2}(\Delta f/Q_{\text{gas}}\omega_0)^{1/2}$

[a]See Ref. 12.
[b]See Ref. 27.
[c]See Ref. 25.
[d]See Ref. 73.
[e]See Ref. 74.
[f]See Ref. 76.
[g]See Ref. 77.

bulk. It may prove quite difficult to achieve ultrahigh Q with such extreme surface-to-volume ratios, if only conventional patterning approaches are utilized. Surface passivation will undoubtedly become imperative for nanometer scale devices.

One might project that structures such as nanotubes and nanowires may well represent the ideal for NEMS, given their perfectly terminated surfaces. So far, however, the existing technology of manipulating, anchoring, and measuring the mechanical properties of nanotube[16,70,71] and nanowire[14,15] devices is still quite primitive. Hence, there is currently insufficient information available even to permit a crude extrapolation of the Qs that might ultimately be attainable at high frequencies with nanotube and nanowire based NEMS.

B. Phase noise

As mentioned above, resonant NEMS devices are envisioned in most initial applications—as high stability oscillators in frequency clocks,[26,27] as highly selective filters in signal processing,[39] and as ultrasensitive sensors.[12] In all of these, the short- and long-term resonance frequency stability of the resonator is central in establishing the operation limits.[72] Here, we turn to a discussion of the phase noise processes and frequency stability in NEMS resonators.

The frequency stability of a resonator–transducer–amplifier cascade (see the discussion in Sec. II F and Fig. 5) is determined by extrinsic processes in the transducer circuitry[27,23] and intrinsic processes fundamental to the resonator itself.[25,38] The frequency stability in macro- and micromechanical resonators have, in most cases to date, been limited by extrinsic elements, such as the transducer–amplifier cascade. In the domain of NEMS, however, given the enhanced sensitivity that is attainable as devices become smaller and as ultrasensitive displacement transduction techniques emerge, fundamental fluctuation processes are increasingly likely to determine the outcome.

In a recent article,[25] Cleland and Roukes have obtained expressions for phase noise in NEMS originating from a variety of intrinsic physical processes. In a subsequent article, Ekinci *et al.*[37] converted the phase noise in Ref. 25 into frequency fluctuations for specific measurement schemes. Later, the formalism was extended to extrinsic processes.[12] Table II summarizes these recent results of the functional forms of the spectral density of the frequency fluctuations (phase noise) $S_\omega(\omega)$ and the corresponding frequency fluctuations $\delta\omega_0 \approx [\int_{2\pi\Delta f} S_\omega(\omega)d\omega]^{1/2}$ for these processes. In the first row of Table II, amplifier transducer dominated frequency stability is presented. The intrinsic processes considered in the subsequent rows include the thermomechanical noise generated by the internal loss mechanisms in the resonator, temperature fluctuations caused by the finite thermal conductance of the resonator,[25] adsorption–desorption noise,[73–75] and momentum exchange noise[76,77] from surrounding gas molecules.

C. Development of transducers

The rms vibration amplitude for a mechanical device (operating within its linear range) scales downward in direct proportion to its size. In Table I, the critical amplitude $\langle x_c\rangle$ for a number of NEMS devices are displayed. Such miniscule displacement amplitudes indicate that to effectively operate these devices, ultrahigh sensitivity displacement transducers are needed. To couple into the motion of NEMS devices in ultrafast applications, a large operation bandwidth

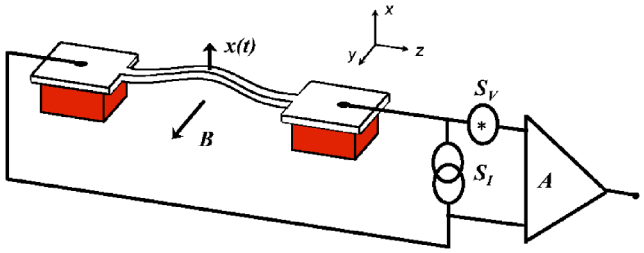

FIG. 8. (Color online). Magnetomotive displacement detection scheme. The displacement sensitivity in the text is estimated by assuming that the dominant source of noise is the noise generated in the first stage amplifier.

is essential. Orthogonality of actuation and transduction ports, i.e., having input and output ports that strongly interact with the mechanical element but with only weak direct couplings to each other, is another desirable property.

The mainstay displacement detection in the domain of MEMS is through electronic and optical coupling. Electronically coupled displacement detection in MEMS has been successfully realized using magnetic,[78] electrostatic,[79] piezoelectric,[80] and piezoresistive[81] transducers. In optical MEMS devices, optical interferometry[82] and optical beam deflection[83] techniques have been successfully used. Both approaches, however, become quickly insensitive at the reduced dimensions of NEMS. The major problem in electronic coupling is that, as the device size shrinks and the frequency of operation increases, the motional modulation of the impedance becomes progressively smaller—while the parasitic embedding impedances continue to grow. The attractive electronic two-port actuation–detection configuration of most MEMS devices becomes hard to realize at the scale of NEMS, due to the unavoidable stray couplings encountered at the reduced dimensions of NEMS. On the other hand, optical displacement detection in small structures is limited by the diffraction of light.

Among the most needed elements for developing NEMS based technologies are broadband, on-chip transduction methods sensitive to subnanometer displacements. It has been rather challenging to implement displacement detection schemes with the aforementioned attributes. A variety of techniques appear to hold promise for NEMS. Below, we shall discuss in some detail some of these transduction schemes and evaluate the promise they hold.

A displacement detection scheme that scales well into the NEMS domain and offers direct electronic coupling to the NEMS displacement is magnetomotive detection.[2,52] It is based upon the presence of a uniform static field, through which a conducting nanomechanical element (usually a nanomechanical doubly clamped beam in a conducting loop) is moved. A schematic of magnetomotive detection is shown in Fig. 8. Usually, the beam element is driven by a Lorentz force, generated by passing an ac current through it in the static magnetic field. The time-varying flux generates an induced electromotive force in the loop. For a doubly clamped beam (see Fig. 3), the responsivity of the magnetomotive transduction can be evaluated as $|\Re| = |\partial V/\partial X| = \xi l B \omega$, where B is the magnetic field strength and l is the length of the beam; here, the midpoint of the beam displaces at a frequency ω. ξ is a geometric factor and $\xi \approx 0.885$. Using Fig. 8 and the concepts developed in Sec. II F, one can obtain an amplifier limited displacement sensitivity for the scheme as

$$[S_X(\omega)]^{1/2} = \left(\frac{S_V(\omega)}{(\xi l B \omega)^2} + \frac{S_I(\omega) l^2 B}{M_{\mathrm{eff}}^2 [(\omega^2 - \omega_0^2)^2 + \omega^2 \omega_0^2 / Q^2]^2} \right)^{1/2}.$$

Here, $S_V(\omega)$ and $S_I(\omega)$ are the voltage and current noise spectral density of the amplifier, respectively.

By employing optical interferometry, shot noise limited displacement sensitivities $S_X^{1/2} \sim 10^{-6}$ nm/$\sqrt{\mathrm{Hz}}$ are routinely attainable on objects with cross sections larger than the diffraction limited optical spot.[82,84] Recently, optical interferometry techniques, in particular path stabilized Michelson interferometry and Fabry–Pérot interferometry, have been extended into the NEMS domain.[85–89] Figure 9 shows a typical room temperature optical interferometer setup. In path

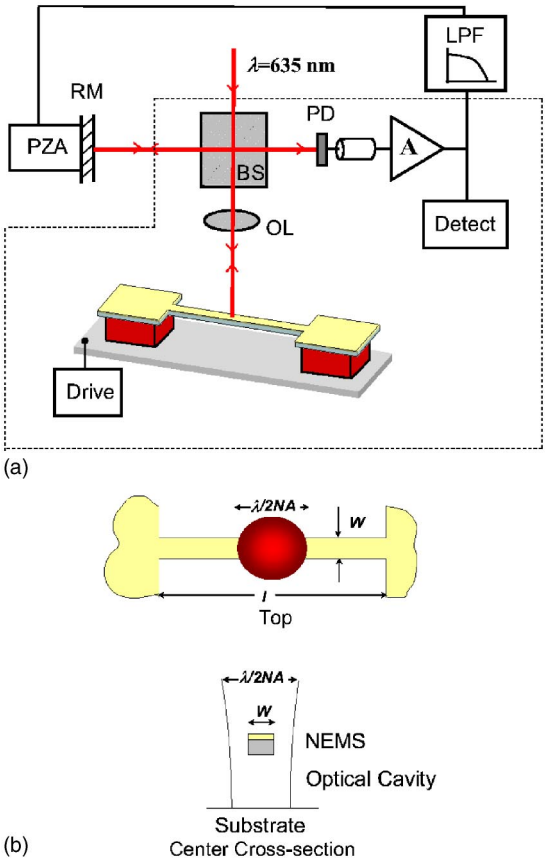

FIG. 9. (Color online). (a) Schematic diagram of the free space optical setup in use at Boston University (see Ref. 89). The optical interferometer is mounted on a *XYZ* translation stage (not shown). The interferometer comprises various beamsplitters (BSs), a reference mirror (RM), and a photodetector (PD). The probe beam used for NEMS displacement detection is tightly focused on the device by a 50× objective lens (OL) with numerical aperture (NA=0.5). The light reflecting from the NEMS is collected by the same lens and interferes with the reference beam on the PD. A constant reference path length is maintained by using a low-pass filter (LPF) and a piezoelectric actuator (PZA). The dashed line indicates the portion of the setup used for the Fabry–Perot cavity measurements; the reference arm of the optics is simply blocked in the measurements. (b) Top view and center cross section of a doubly clamped NEMS beam in relation to the optical spot with Gaussian profile.

stabilized Michelson interferometry, a tightly focused laser beam reflects from the surface of a NEMS device and interferes with a reference beam. In the case of Fabry–Pérot interferometry, the optical cavity formed in the sacrificial gap of a NEMS—between the NEMS surface and the substrate—modulates the optical signal [Fig. 9(b)]. In both techniques strong diffraction effects emerge[89] as the relevant NEMS dimensions are reduced beyond the optical wavelength used. Consequently, shot noise limited displacement sensitivities demonstrated on larger objects are not easily achievable on NEMS. Possibilities, however, do exist for integrated[90] and near-field optical displacement sensors. In particular, solid immersion lens microscopy[91] and tip enhancement[92] techniques appear to hold promise.

In electrostatic transduction, dynamical capacitance changes due to NEMS motion—on the order of 10^{-18} F—are obscured by parasitic capacitances that are many orders of magnitude larger. There may be an escape from this spiral of decreasing motional impedance accompanied by increasing parasitics that occur when device size is scaled downward. The solution would be to eliminate the large embedding and parasitic impedances. A balanced bridge technique,[10] for instance, has been shown to reduce the resistive and capacitive backgrounds. Impedance matching techniques might also offer remedies.[93] One could also locate a subsequent amplification stage (which would, in effect, act as an impedance transformer/line driver) directly at the capacitive transducer. Recently, a single-electron-transistor (SET) has been integrated to a NEMS resonator[69,94] with the NEMS electrode serving a dual purpose—as both motion sensor for the NEMS, and as gate electrode of the SET readout.[95,96]

Piezoelectric displacement transduction can be realized by detecting the time-varying polarization fields created by local time-varying strain fields within a piezoelectric medium (e.g., at points of high strain within a mechanical resonator). These polarization fields can be detected by placing the gate of a field effect transistor[97] or a single electron transistor[98] where the time-varying electric polarization is largest. Suspended high mobility electron structures have also been exploited in the piezoelectric detection of nanoscale motion.[4,99] Piezoresistive detection[100] is closely related to the piezoelectric detection scheme.

Electron tunneling is a technique that scales well, even down to extremely small dimensions.[101,102] However, because the impedance of a tunnel junction is quite high, the bandwidth of such detectors is minimal in the presence of unavoidable parasitic capacitance. We emphasize that these bandwidth shortcomings are due to technological reasons, not fundamental ones. Quantum mechanical electron tunneling in an atomic scale junction is an inherently fast phenomenon with speeds much greater than 1 GHz.[103] The nonlinear dependence of the tunnel current upon the tunnel gap may prove extremely useful for down conversion schemes[100,104] in high frequency NEMS.

D. Reproducible nanofabrication

Surface nanomachining processes produce NEMS devices with large error margins in fundamental device parameters—even when identical processing parameters are employed.[9,10] This, in part, is an adverse consequence of the miniscule NEMS effective masses (see Table I). Device trimming is ubiquitous in quartz frequency control technology. It is clear that such techniques will also be required for NEMS.

IV. AN EMERGING APPLICATION

Even at this early stage of development, it seems clear that NEMS will ultimately find use in a broad range of applications. Recent demonstrations of NEMS based electrometry,[105] optomechanical,[106] and electromechanical signal processing,[107] and mass detection[12,108–111] have attracted much attention. From a fundamental science point of view, NEMS are opening up investigations of phonon mediated mechanical processes[112–115] and of the quantum behavior of mesoscopic mechanical systems.[69,94,116] In the remainder of this section, we shall focus on a particular NEMS application: nanoelectromechanical mass detection. Our discussion of NEMS based mass detection has several different facets. First, it outlines the ubiquitous resonant sensing concept. Second, it puts NEMS based mass detection into perspective by demonstrating its sensitivity limits. Third, it proposes avenues for NEMS based mass spectrometry.

Resonant mass sensors operate by providing a frequency shift $\delta\omega$ that is directly proportional to the inertial mass δm of the analyte accreted upon them. Given the mass responsivity $\Re_M = \partial\omega_0/\partial M_{\text{eff}}$, δm can be determined as

$$\delta m \approx \left| \frac{\partial M_{\text{eff}}}{\partial \omega_0} \right| \delta\omega = |\Re_M|^{-1} \delta\omega. \tag{5}$$

Here, we assume that the system parameters are weakly coupled for small changes, i.e., $\partial M_{\text{eff}}/\partial \kappa_{\text{eff}} \approx 0$. We can further determine that $\Re_M = -(\omega_0/2M_{\text{eff}})$, and

$$\delta m \approx 2\frac{M_{\text{eff}}}{\omega_0}\delta\omega. \tag{6}$$

Mass sensors with exquisite mass sensitivities based upon the simple relation described by Eq. (6) have been demonstrated and employed in many diverse fields of science and technology. Among the most sensitive are those based upon the acoustic vibratory modes of crystals,[117,118] thin films,[119] and micron-sized cantilevers.[120–122] In all of these, the effective vibratory mass of the resonator M_{eff} and the minimum resolvable frequency shift $\delta\omega_{\text{min}}$ by the measurement circuitry determine the ultimate mass sensitivity δm_{min}. The minuscule M_{eff} of NEMS (see Table I), in conjunction with their high Qs, translates into opportunities for unprecedented mass sensitivity at high operational (resonance) frequencies—as demonstrated in our recent experiments.[12]

Here, we shall briefly review these experiments in an effort to facilitate further discussion. These initial experiments[12] were carried out in a cryogenic UHV environment ($T \approx 17$ K) within the apparatus depicted in Fig. 10(a). This system allows the operation of a magnetomotively transduced NEMS resonator while a pulsed, weak, ballistic flux of Au atoms is directed upon it. Nanomechanical SiC doubly clamped beam resonators, shown in Fig. 10(b), were used as the sensor elements in these experiments. The fun-

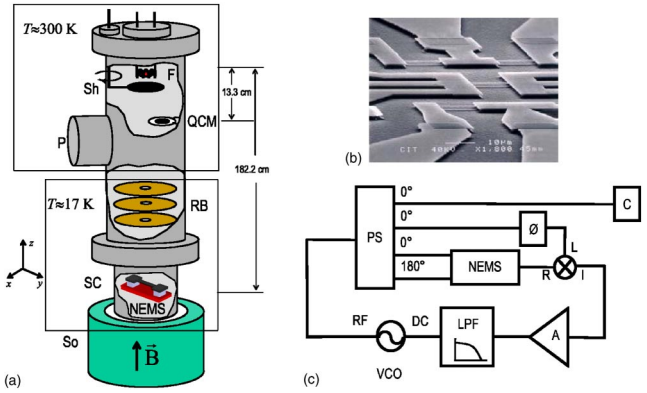

FIG. 10. (Color online). (a) Variable temperature, UHV microwave cryostat for NEMS mass sensitivity measurements. The sample chamber (SC) is inserted into the bore of a 6 T superconducting solenoid (So) in liquid helium. The radiation baffles (RB) establish a line of sight along the z axis from a room temperature thermal Au evaporation source (F) to the bottom of the cryostat. The NEMS resonators are carefully placed in this line-of-sight, some $r_{\mathrm{NEMS}}=182.2$ cm away from this thermal-evaporation source. A calibrated quartz crystal monitor (QCM) at a distance of $r_{\mathrm{QCM}}=13.3$ cm and a room temperature shutter (Sh) are employed to determine and modulate the Au atom flux, respectively. With knowledge of the exposed NEMS surface area A (determined from careful scanning electron microscopy measurements), and the mass flux Φ of the evaporator as measured by the QCM, one can determine the exact mass of the adsorbed Au atoms on the NEMS as $\delta m(t)\approx\int_0^t A\Phi(r_{\mathrm{QCM}}/r_{\mathrm{NEMS}})^2 dt$. In this system, the geometric factor is $(r_{\mathrm{QCM}}/r_{\mathrm{NEMS}})^2\approx 5\times 10^{-3}$. (b) Scanning electron micrographs of nanomechanical doubly clamped beam sensor elements. (c) Conceptual diagram of the phase-locked loop NEMS readout. The principal components are: voltage controlled radio frequency oscillator (VCO); four-port power splitter (PS) (with three 0° and one 180° output ports); NEMS mass sensor with radio frequency bridge readout; mixer (M); phase shifter (Ø); variable gain amplifier (A); and low pass filter (LPF); frequency counter (C).

damental in-plane flexural resonance frequency $\omega_0/2\pi$ of one of the beams was tracked continuously by the phase-locked loop (PLL) circuit shown schematically in Fig. 10(c). In Fig. 11, the temporal evolution of $\omega_0(t)/2\pi$ is displayed, as the beam is exposed to the ballistic flux of Au atoms, changing M_{eff} by an amount $\delta m(t)$. For this system, $\Re_M^{-1}=\partial M_{\mathrm{eff}}/\partial\omega_0$ was deduced to be $|2\pi\Re_M^{-1}|\approx 3.90\times 10^{-19}$ g/Hz. The noise floor of the measurement was determined from the regions of constant frequency when the shutter was closed. For this experiment, a measurement bandwidth of $\Delta f\sim 3$ kHz ($\tau\sim 2$ ms) yielded a frequency noise floor $\delta\omega_{\mathrm{min}}/2\pi\approx 6.51$ Hz—corresponding to a minimum detectable mass $\delta m_{\mathrm{min}}=|\Re_M^{-1}|\delta\omega_{\mathrm{min}}\approx 2.53\times 10^{-18}$ g $\approx 1.5\times 10^6$ Da.[123]

Figure 12 displays extended measurements of mass responsivity obtained from experiments with other representative NEMS devices of varying dimensions and resonance frequencies. As the size of the NEMS sensor is reduced, the mass responsivity increases dramatically, as detailed in Table III. These experiments along with recent calculations[37] clearly demonstrate the potential that NEMS devices offer for mass sensing. The mass sensitivity attainable by NEMS in the near future spans the regime from a few tenths, to a few tens of Daltons. This is the mass range for a small individual molecule, indicating the immense potential for NEMS-based mass spectrometry. In addition, NEMS could provide powerful approaches to biothreat detection, drug screening, and medical diagnostics—all with sensitivity at the single molecule level.

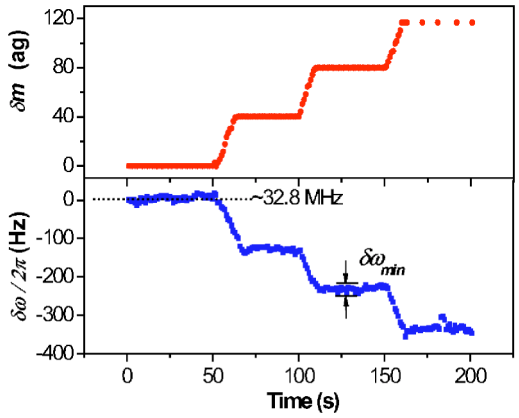

FIG. 11. (Color online). Frequency shifts $\delta\omega/2\pi$ (bottom) induced by sequential 40 attogram (ag) (1 ag$=10^{-18}$ g) gold atom adsorption upon a 670 nm$\times$259 nm$\times$14.2 μm silicon carbide doubly clamped beam resonator. The (initial) fundamental frequency is $\omega_0/2\pi\approx 32.8$ MHz. The accreted mass of gold atoms δm in the upper plot is measured by a separate quartz crystal detector. The rms frequency fluctuations of the system (i.e., the noise level in the lower trace) correspond to a mass sensitivity of $\delta m_{\mathrm{min}}\approx 2.5$ ag for the 2 ms averaging time employed. δm_{min} for this system appears to be limited by the noise in the transducer–amplifier cascade, i.e., $\delta m_{\mathrm{min}}\sim(2M_{\mathrm{eff}}/Q)10^{-(\mathrm{DR}/20)}$ obtained upon setting $\delta\omega_{\mathrm{min}}\sim(\omega_0/Q)10^{-(\mathrm{DR}/20)}$ [see Table II and Eq. (6)]. The system parameters determined from separate measurements were $Q\approx 3000$, DR≈ 60 dB, and $M_{\mathrm{eff}}\approx 7\times 10^{-12}$ g. This leads to the approximate result that $\delta m_{\mathrm{min}}\approx 1$ ag—quite close to what we experimentally attain.

With attainment of single-Dalton mass resolution, NEMS based mass spectrometry will offer possibilities for mass spectrometry of individual macromolecules. In such an implementation, a very low flux beam of neutral, gas phase species of the analyte would impinge and adhere to a NEMS resonator. Individually resolved jumps in the resonance frequency of the NEMS device would then directly indicate the mass of these adsorbing molecules. This approach offers the unique capability of mass spectrometry of individual neutral species. We note that an inherent and important limitation of current mass spectrometry techniques is that the absolute mass itself is not accessible, but instead it is the mass-to-charge ratio that is obtained.

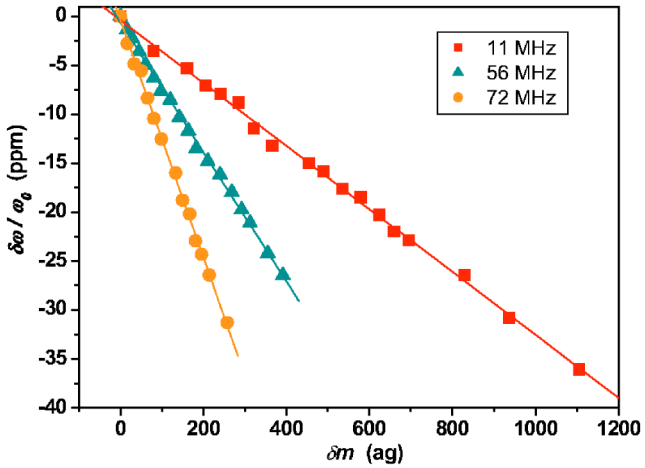

FIG. 12. (Color online). Data from three additional SiC devices with $\omega_0/2\pi\approx 11$, 56, and 72 MHz displayed with linear fits. The measured and calculated device properties are presented in Table III.

TABLE III. Calculated and experimental values of the mass responsivity in doubly clamped beam resonators.

$\omega_0/2\pi$ (MHz)	$w\times t\times l$ (μm)	M_{tot} (g)	$[\lvert\Re_M\rvert/(2\pi)]_{\text{calc}}$ (Hz/ag)	$[\lvert\Re_M\rvert/(2\pi)]_{\text{expt}}$ (Hz/ag)
11.4	$0.8\times0.26\times26.2$	36×10^{-12}	0.22	0.50
32.8	$0.67\times0.26\times14$	9.9×10^{-12}	2.2	2.6
56	$0.65\times0.26\times12$	7.1×10^{-12}	5.2	5.1
72	$0.65\times0.26\times10$	6.0×10^{-12}	8.2	12

Even before single-Dalton resolution is attained, NEMS can provide significant enhancement of conventional mass spectrometry, if employed as detectors in currently available mass spectrometers.[124] In such an implementation, the analyte molecules would be ionized and mass separated by conventional techniques.[125] The ions would then be directed upon a NEMS sensor element, capable of registering single ion adsorption events. An arbitrarily large mass resolution—much smaller than the δm_{min} allowed by the system—could be achievable through signal averaging. With the $\delta m_{\text{min}} \sim 1$ MDa demonstrated here, for instance, after sequential deposition of $N\sim10^6$ individual 1 MDa species, it would be possible to obtain single Dalton resolution. In NEMS detection, the minimum temporal separation between individual molecular sensing events would be determined by the averaging time required to establish the instantaneous frequency to the desired measurement accuracy. The 2 ms averaging time (see Fig. 11) would yield the above-mentioned 1 Da sensitivity for a $\sim$1 MDa species in $\sim$30 m. Finally, the immense mass dynamic range of a NEMS device would be a much desired attribute in mass spectrometry.

V. OUTLOOK

NEMS offer access to a parameter space for sensing and fundamental measurements that is unprecedented and intriguing. Taking full advantage of NEMS will stretch our collective imagination, as well as our current methods and "mindsets" in micro- and nanodevice science and technology. It seems certain that many applications will emerge from this new field. Ultimately, the nanomechanical systems outlined here will yield to true nanotechnology. By the latter we envisage reproducible techniques allowing mass production of devices of arbitrary complexity, that comprise, say, a few million atoms—each of which is placed with atomic precision.[126] Clearly, realizing the "Feynmanesque" dream will take much sustained effort in a host of laboratories. Meanwhile, NEMS, as outlined here, can today provide the crucial scientific and engineering foundation that will underlie this future nanotechnology.

ACKNOWLEDGMENTS

K.L.E. is grateful to the NSF for support under Grant Nos. CMS-0324416, DMR-0315662, BES-0216274, and ECS-0210752. M.L.R. acknowledges support from DARPA/MTO, SPAWAR, and the NSF under Grant No. ECS-0089061.

[1] M. L. Roukes, Phys. World **14**, 25 (2001).
[2] A. N. Cleland and M. L. Roukes, Appl. Phys. Lett. **69**, 2653 (1996).
[3] D. W. Carr, S. Evoy, L. Sekaric, H. G. Craighead, and J. M. Parpia, Appl. Phys. Lett. **75**, 920 (1999).
[4] R. H. Blick, M. L. Roukes, W. Wegscheider, and M. Bichler, Physica B **249–251**, 784 (1998).
[5] Y. T. Yang, K. L. Ekinci, X. M. H. Huang, L. M. Schiavone, C. Zorman, M. Mehregany, and M. L. Roukes, Appl. Phys. Lett. **78**, 162 (2001).
[6] A. N. Cleland, M. Pophristic, and I. Ferguson, Appl. Phys. Lett. **79**, 2070 (2001).
[7] L. Sekaric *et al.*, Appl. Phys. Lett. **81**, 4455 (2002).
[8] L. Sekaric, D. W. Carr, S. Evoy, J. M. Parpia, and H. G. Craighead, Sens. Actuators, A **101**, 215 (2002).
[9] X. M. H. Huang, C. Zorman, M. Mehregany, and M. L. Roukes, Nature (London) **421**, 496 (2003).
[10] K. L. Ekinci, Y. T. Yang, X. M. Huang, and M. L. Roukes, Appl. Phys. Lett. **81**, 2253 (2002).
[11] M. L. Roukes, Physica B **263–264**, 1 (1999).
[12] K. L. Ekinci, X. M. H. Huang, and M. L. Roukes, Appl. Phys. Lett. **84**, 4469 (2004).
[13] A. Cleland, *Foundations of Nanomechanics* (Springer, New York, 2003).
[14] M. F. Yu, G. J. Wagner, R. S. Ruoff, and M. J. Dyer, Phys. Rev. B **66**, 073406 (2002).
[15] A. Husain, J. Hone, H. W. C. Postma, X. M. H. Huang, T. Drake, M. Barbic, A. Scherer, and M. L. Roukes, Appl. Phys. Lett. **83**, 1240 (2003).
[16] V. Sazonova, Y. Yaish, H. Ustunel, D. Roundy, T. A. Arias, and P. L. McEuen, Nature (London) **431**, 284 (2004).
[17] J. Q. Broughton, C. A. Meli, P. Vashishta, and R. K. Kalia, Phys. Rev. B **56**, 611 (1997).
[18] R. Phillips, *Crystals, Defects and Microstructures* (Cambridge University Press, Cambridge, 2001).
[19] X. Li, T. Ono, Y. Wang, and M. Esashi, Appl. Phys. Lett. **83**, 3081 (2003).
[20] C. T.-C. Nguyen, L P. B. Katehi, and G. M. Rebeiz, Proc. IEEE **86**, 1756 (1998).
[21] J. L. Garbini, K. J. Bruland, W. M. Dougherty, and J. A. Sidles, J. Appl. Phys. **80**, 1951 (1996).
[22] K. J. Bruland, J. L. Garbini, W. M. Dougherty, and J. A. Sidles, J. Appl. Phys. **83**, 3972 (1998).
[23] T. R. Albrecht, P. Grutter, D. Horne, and D. Rugar, J. Appl. Phys. **69**, 668 (1991).
[24] V. B. Braginsky and F. Y. Khalili, *Quantum Measurement* (Cambridge University Press, Cambridge, 1992).
[25] A. N. Cleland and M. L. Roukes, J. Appl. Phys. **92**, 2758 (2002).
[26] F. L. Walls and J. Vig, IEEE Trans. Ultrason. Ferroelectr. Freq. Control **42**, 576 (1995).
[27] W. P. Robins, *Phase Noise in Signal Sources* (Peter Pelegrinus Ltd., London, 1982).
[28] A. H. Nayfeh and T. R. Mook, *Nonlinear Oscillations* (Wiley Interscience, New York, 1979).
[29] L. D. Landau and E. M. Lifshitz, *Theory of Elasticity* (Pergamon Press, Oxford, 1959).
[30] H. A. C. Tilmans, M. Elwenspoek, and H. J. Flutiman, Sens. Actuators, A **30**, 35 (1992).
[31] V. Kaajakari, T. Mattila, A. Oja, and H. Seppa, J. Microelectromech. Syst. **13**, 715 (2004).
[32] D. S. Greywall, B. Yurke, P. A. Busch, A. N. Pargellis, and R. L. Willett, Phys. Rev. Lett. **72**, 2992 (1994).
[33] K. L. Turner *et al.*, Nature (London) **396**, 149 (1998).
[34] D. W. Carr, S. Evoy, L. Sekaric, H. G. Craighead, and J. M. Parpia, Appl. Phys. Lett. **77**, 1545 (2000).
[35] D. V. Scheible, A. Erbe, and R. H. Blick, and G. Corso, Appl. Phys. Lett. **81**, 1884 (2002).
[36] R. Lifshitz and M. C. Cross, Phys. Rev. B **67**, 134302 (2003).
[37] K. L. Ekinci, Y. T. Yang, and M. L. Roukes, J. Appl. Phys. **95**, 2682 (2004).
[38] J. R. Vig and Y. Kim, IEEE Trans. Ultrason. Ferroelectr. Freq. Control **46**,1558 (1999).
[39] K. Wang and C. T.-C. Nguyen, Proceedings, 1997 IEEE International Micro Electro Mechanical Systems Workshop, Nagoya, Japan, Jan. 26–30, 1997, pp. 25–30.
[40] T. D. Stowe, K. Yasumura, T. W. Kenny, D. Botkin, K. Wago, and D. Rugar, Appl. Phys. Lett. **71**, 288 (1997).
[41] M. M. Midzor *et al.*, J. Appl. Phys. **87**, 6493 (2000).
[42] K. Kokubun, M. Hirata, M. Ono, H. Murakami, and Y. Toda, J. Vac. Sci. Technol. A **5**, 2450 (1987).

[43] F. R. Blom, S. Bouwstra, M. Elwenspoek, and J. H. J. Fluitman, J. Vac. Sci. Technol. B **10**, 19 (1992).
[44] K. Yum *et al.*, J. Appl. Phys. **96**, 3933 (2004).
[45] R. B. Bhiladvala and Z. J. Wang, Phys. Rev. E **69**, 036307 (2004).
[46] L. D. Landau, *Fluid Mechanics* (Pergamon, Oxford, 1982).
[47] V. B. Braginsky, V. P. Mitrofanov, and V. I. Panov, *Systems with Small Dissipation* (The University of Chicago Press, Chicago, 1985).
[48] M. C. Cross and R. Lifshitz, Phys. Rev. B **64**, 085324 (2001).
[49] D. M. Photiadis and J. A. Judge, Appl. Phys. Lett. **85**, 482 (2004).
[50] H. Jiang, M.-F. Yu, B. Liu, and Y. Huang, Phys. Rev. Lett. **93**, 185501 (2004).
[51] X. M. H. Huang, M. K. Prakash, C. A. Zorman, M. Mehregany, and M. L. Roukes, TRANSDUCERS '03 Proceedings 12th International Conference on Solid State Sensors, Actuators and Microsystems, Boston, June 8–12, 2003.
[52] A. N. Cleland and M. L. Roukes, Sens. Actuators, A **72**, 256 (1999).
[53] K. C. Schwab, Appl. Phys. Lett. **80**, 1276 (2002).
[54] R. Lifshitz and M. L. Roukes, Phys. Rev. B **61**, 5600 (2000).
[55] A. B. Hutchinson, P. A. Truitt, K. C. Schwab, L. Sekaric, J. M. Parpia, H. G. Craighead, and J. E. Butler, Appl. Phys. Lett. **84**, 972 (2004).
[56] S. Evoy, A. Olkhovets, L. Sekaric, J. M. Parpia, H. G. Craighead, and D. W. Carr, Appl. Phys. Lett. **77**, 2397 (2000).
[57] K. Y. Yasumura, T. D. Stowe, E. M. Chow, T. Pfafman, T. W. Kenny, B. C. Stipe, and D. Rugar, J. Microelectromech. Syst. **9**, 117 (2000).
[58] K. Y. Yasumura, T. D. Stowe, E. M. Chow, T. Pfafman, T. W. Kenny, and D. Rugar, *Proceedings Technical Digest of the 1998 Solid-State Sensor and Actuator Workshop*, Hilton Head Island, SC, June 8–11, 1998 (Transducer Research Foundation, Cleveland, 1998).
[59] J. Yang, T. Ono, and M. Esashi, Appl. Phys. Lett. **77**, 3860 (2000).
[60] J. Yang, T. Ono, and M. Esashi, J. Vac. Sci. Technol. B **19**, 551 (2001).
[61] Y. Wang, J. A. Henry, D. Sengupta, and M. A. Hines, Appl. Phys. Lett. **85**, 5736 (2004).
[62] D. F. Mcguigan, C. C. Lam, R. Q. Gram, A. W. Hoffman, D. H. Douglass, and H. W. Gutche, J. Low Temp. Phys. **30**, 621 1978.
[63] R. N. Kleiman, G. Agnolet, and D. J. Bishop, Phys. Rev. Lett. **59**, 2079 (1987).
[64] T. Klistner and R. O. Pohl, Phys. Rev. B **36**, 6551 (1987).
[65] William Duffy, Jr., J. Appl. Phys. **68**, 5601 (1990).
[66] R. A. Buser and N. F. de Rooij, Sens. Actuators, A **21**, 323 (1990).
[67] D. S. Greywall, B. Yurke, P. A. Busch, and S. C. Arney, Europhys. Lett. **34**, 37 (1996).
[68] R. E. Mihailovich and J. M. Parpia, Phys. Rev. Lett. **68**, 3052 (1992).
[69] M. D. LaHaye, O. Buu, B. Camarota, and K. C. Schwab, Science **304**, 74 (2004).
[70] H. Dai, Phys. World **13**, 43 (2000).
[71] J. Chung, K.-H. Lee, J. Lee, and R. S. Ruoff, Langmuir **20**, 3011 (2004).
[72] T. H. Lee and A. Hajimiri, IEEE J. Solid-State Circuits **35**, 326 (2000).
[73] Y. K. Yong and J. R. Vig, IEEE Trans. Ultrason. Ferroelectr. Freq. Control **36**, 452 (1989).
[74] Y. K. Yong and J. R. Vig, IEEE Trans. Ultrason. Ferroelectr. Freq. Control **37**, 543 (1990).
[75] D. Enguang, IEEE Trans. Ultrason. Ferroelectr. Freq. Control **49**, 649 (2002).
[76] W. Gerlach, Naturwiss. **15**, 15 (1927).
[77] G. E. Uhlenbeck and S. Goudsmit, Phys. Rev. **34**, 145 (1929).
[78] D. S. Greywall, B. Yurke, P. A. Busch, A. N. Pargellis, and R. L. Willett, Phys. Rev. Lett. **72**, 2992 (1992).
[79] W. C. Tang, T. C. H. Nguyen, M. W. Judy, and R. T. Howe, Sens. Actuators, A **21**, 328 (1990).
[80] J. Soderkvist and K. Hjort, J. Micromech. Microeng. **4**, 28 (1994).
[81] M. Tortonese, R. C. Barret, and C. F. Quate, Appl. Phys. Lett. **62**, 834 (1993).
[82] J. W. Wagner, Phys. Acoust. **19**, 201 (1990).
[83] T. G. Bifano, J. Perreault, R. K. Mali, and M. N. Horenstein, IEEE J. Sel. Top. Quantum Electron. **5**, 83 (1999).
[84] T. R. Albrecht, P. Grütter, D. Rugar, and D. P. E. Smith, Ultramicroscopy **42**, 1638 (1992).
[85] D. W. Carr, L. Sekaric, and H. G. Craighead, J. Vac. Sci. Technol. B **16**, 3821 (1998).
[86] D. W. Carr, S. Evoy, L. Sekaric, A. Olkhovets, J. M. Parpia, and H. G. Craighead, Appl. Phys. Lett. **77**, 1545 (2000).
[87] C. Meyer, H. Lorenz, and K. Karrai, Appl. Phys. Lett. **83**, 2420 (2003).
[88] B. E. N. Keeler, D. W. Carr, J. P. Sullivan, T. A. Friedmann, and J. R. Wendt, Opt. Lett. **29**, 1182 (2004).
[89] T. Kouh, D. Karabacak, D. H. Kim, and K. L. Ekinci, Appl. Phys. Lett. **86**, 013106 (2005).
[90] E. Ollier, IEEE J. Sel. Top. Quantum Electron. **8**, 155 (2002).
[91] S. B. Ippolito, B. B. Goldberg, and M. S. Unlu, Appl. Phys. Lett. **78**, 4071 (2001).
[92] E. J. Sánchez, L. Novotny, and X. S. Xie, Phys. Rev. Lett. **82**, 4014 (1999).
[93] P. A. Truitt, J. Hertzberg, and K. C. Schwab, Bull. Am. Phys. Soc. **50**, 1307 (2005).
[94] R. G. Knobel and A. N. Cleland, Nature (London) **424**, 291 (2003).
[95] M. P. Blencowe, Proc. SPIE **5115**, 64 (2003).
[96] M. P. Blencowe and M. N. Wybourne, Appl. Phys. Lett. **77**, 3845 (2000).
[97] R. G. Beck, M. A. Eriksson, and R. M. Westervelt, Appl. Phys. Lett. **73**, 1149 (1998).
[98] R. Knobel and A. N. Cleland, Appl. Phys. Lett. **81**, 2258 (2002).
[99] H. X. Tang, X. M. H. Huang, M. L. Roukes, M. Bichler, and W. Wegscheider, Appl. Phys. Lett. **81**, 3879 (2002).
[100] I. Bargatin, E. B. Myers, J. Arlett, B. Gudlewski, and M. L. Roukes, Appl. Phys. Lett. **86**, 133109 (2005).
[101] M. F. Bocko, Rev. Sci. Instrum. **61**, 3763 (1990).
[102] T. W. Kenny *et al.*, J. Vac. Sci. Technol. A **10**, 2114 (1992).
[103] G. Nunes, Jr. and M. R. Freeman, Science **262**, 1029 (1993).
[104] A. N. Cleland, J. S. Aldridge, D. C. Driscoll, and A. C. Gossard, Appl. Phys. Lett. **81**, 1699 (2002).
[105] A. N. Cleland and M. L. Roukes, Nature (London) **392**, 160 (1998).
[106] L. Sekaric, M. Zalalutdinov, S. W. Turner, A. T. Zehnder, J. M. Parpia, and H. G. Craighead, Appl. Phys. Lett. **80**, 3617 (2002).
[107] A. Erbe, H. Krömmer, A. Kraus, R. H. Blick, G. Corso, and K. Richter, Appl. Phys. Lett. **77**, 3102 (2000).
[108] M. L. Roukes and K. L. Ekinci, U. S. Patent 6,722,200 (20 April 2004).
[109] B. Ilic, H. G. Craighead, S. Krylov, W. Senaratne, C. Ober, and P. Neuzil, J. Appl. Phys. **95**, 3694 (2004).
[110] N. V. Lavrik and P. G. Datskos, Appl. Phys. Lett. **82**, 2697 (2003).
[111] A. Gupta, D. Akin, and R. Bashir, Appl. Phys. Lett. **84**, 1976 (2004).
[112] T. S. Tighe, J. M. Worlock, and M. L. Roukes, Appl. Phys. Lett. **70**, 2687 (1997).
[113] K. C. Schwab, E. A. Henriksen, J. M. Worlock, and M. L. Roukes, Nature (London) **404**, 974 (2000).
[114] C. S. Yung, D. R. Schmidt, and A. N. Cleland, Appl. Phys. Lett. **81**, 31 (2002).
[115] W. Fon *et al.*, Phys. Rev. B **66**, 045302 (2002).
[116] M. Blencowe, Phys. Rep. **395**, 159 (2004).
[117] C. Lu, *Applications of Piezoelectric Quartz Crystal Microbalances* (Elsevier, London, 1984).
[118] S. S. Narine and A. J. Slavin, J. Vac. Sci. Technol. A **16**, 1857 (1998).
[119] M. Thompson and D. C. Stone, *Surface-Launched Acoustic Wave Sensors: Chemical Sensing and Thin-Film Characterization* (Wiley, New York, 1997).
[120] T. Thundat, E. A. Wachter, S. L. Sharp, and R. J. Warmack, Appl. Phys. Lett. **66**, 1695 (1995).
[121] B. Ilic *et al.*, Appl. Phys. Lett. **77**, 450 (2000).
[122] Z. J. Davis *et al.*, J. Vac. Sci. Technol. B **18**, 612 (2000).
[123] The SI defines 1 Da as 1/12 the mass of the C^{12} atom. 1 Da = 1.66×10^{-27} kg
[124] W. K. Hibert, X. L. Feng, and M. L. Roukes, Am. Phys. Soc. **50**, 1132 (2005).
[125] E. de Hoffmann and V. Stroobant, *Mass Spectrometry Principles and Applications* (Wiley, New York, 2002).
[126] R. P. Feynman, *Proceeding of American Physical Society Meeting*, Pasadena, CA, December 29, 1959 (originally published in Caltech's *Engineering and Science magazine*, Feb. 1960); reprinted as R. P. Feynman, J. Microelectromech. Syst. **2**, 1 (1993).